

## Article

# Application Study on the Activated Coke for Mercury Adsorption in the Nonferrous Smelting Industry

Yang Zheng <sup>1,2</sup>, Guoliang Li <sup>1,2,\*</sup>, Jiayan Jiang <sup>1</sup>, Lin Zhang <sup>1</sup> and Tao Yue <sup>1,2,\*</sup>

<sup>1</sup> School of Energy and Environmental Engineering, University of Science and Technology Beijing, Beijing 100083, China; yzheng@ustb.edu.cn (Y.Z.); u202141298@xs.ustb.edu.cn (J.J.); m202220218@xs.ustb.edu.cn (L.Z.)

<sup>2</sup> Beijing Key Laboratory on Resource-Oriented Treatment of Industrial Pollutants, Beijing 100083, China

\* Correspondence: liguoliang@ustb.edu.cn (G.L.); yuetao@ustb.edu.cn (T.Y.)

**Abstract:** The massive release of mercury undermines environmental sustainability, and with the official entry into force of the Minamata Convention, it is urgent to strengthen the control of mercury pollution. The effectiveness of activated coke (AC) in removing elemental mercury (Hg<sup>0</sup>) from high temperatures and sulfur nonferrous smelting flue gas before acid production was studied. Experimental results indicated that the optimal temperature for Hg<sup>0</sup> adsorption by AC was 150 °C. And the adsorption of Hg<sup>0</sup> by AC was predominantly attributed to physical adsorption. Flue gas components (SO<sub>2</sub> and O<sub>2</sub>) impact studies indicated that O<sub>2</sub> did not significantly affect Hg<sup>0</sup> adsorption compared to pure N<sub>2</sub>. Conversely, SO<sub>2</sub> suppressed the adsorption capacity, while the simultaneous presence of SO<sub>2</sub> and O<sub>2</sub> exhibited a synergistic effect in facilitating the removal of Hg<sup>0</sup>. The characterization results of X-ray photoelectron spectroscopy (XPS) indicated that the SO<sub>2</sub> molecule favored to anchor at the O<sub>α</sub> site, leading to the formation of SO<sub>3</sub>. This subsequently oxidized the mercury to HgSO<sub>4</sub> instead of HgO. The study demonstrates that cheap and easily accessible AC applications in the adsorption of mercury technology may help improve the sustainability of the circular economy and positively impact various environmental aspects.

**Keywords:** activated coke; mercury capture; nonferrous smelting; sustainability



**Citation:** Zheng, Y.; Li, G.; Jiang, J.; Zhang, L.; Yue, T. Application Study on the Activated Coke for Mercury Adsorption in the Nonferrous Smelting Industry. *Sustainability* **2024**, *16*, 421. <https://doi.org/10.3390/su16010421>

Academic Editor: Grigorios L. Kyriakopoulos

Received: 28 November 2023

Revised: 26 December 2023

Accepted: 28 December 2023

Published: 3 January 2024



**Copyright:** © 2024 by the authors. Licensee MDPI, Basel, Switzerland. This article is an open access article distributed under the terms and conditions of the Creative Commons Attribution (CC BY) license (<https://creativecommons.org/licenses/by/4.0/>).

## 1. Introduction

Mercury is persistent, bioaccumulated, and can be transported long distances, seriously jeopardizing the ecological environment and human health [1,2]. In 2015, approximately 2220 t Hg was emitted into the atmosphere from 17 key industries globally, 49% of which was articulated by Asia (mainly east and southeast Asia). Nonferrous smelting Hg emissions accounted for 15% of the total emissions in Asia, which severely impacted the environment [3]. Moreover, China is the most significant anthropogenic mercury emitting country, with national mercury emissions reaching 530 t in 2014, and 84% of the non-coal-fired atmospheric mercury emissions originated from nonferrous smelting [4]. The increasing prominence of mercury pollution is detrimental to global sustainable development, so there has become more and more of a consensus to strengthen the prevention and control of mercury pollution, and it is of great significance to control mercury emissions from the nonferrous smelting industry [5,6].

The primary application of nonferrous smelting flue gas mercury removal technology occurs post-flue gas scrubbing. The nonferrous smelting industry's acid manufacturing process exhibits favorable mercury absorption properties. However, suppose mercury is not eliminated prior to the acid manufacturing process. In that case, a considerable quantity of mercury may infiltrate the contaminated acid, acid sludge, and other mediums, leading to additional contamination during subsequent utilization. Consequently, the nonferrous smelting industry generates a substantial mercury discharge, significantly affecting the acid production process. Therefore, it's of great necessity to remove mercury before the

acid production process [7]. Hence, it is imperative to eliminate mercury prior to the acid production procedure. Nevertheless, the nonferrous smelting flue gas exhibits notable attributes such as elevated mercury concentration, high SO<sub>2</sub> concentration, and elevated flue gas temperature, posing challenges for conventional adsorption materials in effectively extracting mercury from the flue gas [6,7].

Activated coke (AC) holds promise for mercury removal in the nonferrous industry owing to its abundant availability, cost-effectiveness, ease of access, commendable resistance to sulfur, and the superior stability of its adsorption products [8]. The primary distinction between conventional activated carbon and AC lies in the broader distribution of pore sizes in AC, encompassing micropores, mesopores, and numerous macropores. Consequently, the adsorption rate of AC is accelerated [9,10]. Furthermore, AC exhibits superior mechanical strength and abrasion resistance compared to activated carbon, enabling it to maintain stability and resist damage or deactivation even in conditions of high temperature, high pressure, and strong oxidants. Research has demonstrated that the impact of SO<sub>2</sub> on Hg<sup>0</sup> adsorption varies under different circumstances [11], sometimes showing inhibition and sometimes promotion. Hence, the meticulous selection of materials is paramount in preparing adsorbents. While there exists a plethora of research on AC desulfurization and denitrification, the investigation of AC as an adsorbent for eliminating high-temperature and high-sulfur flue gas monomers of mercury remains relatively limited.

In order to improve the adsorption performance of active coke, researchers modified the adsorbent with Mn, Ce, Cu, Co, and other metal compounds, and explored the mechanism of mercury removal [12–15]. However, the existing studies are mainly focused on the flue gas from coal-fired industries. Moreover, the understanding of the interaction between Hg<sup>0</sup> and SO<sub>2</sub> on the surface of AC is lacking. Therefore, it is imperative to conduct a comprehensive analysis of the adsorption properties of AC for mercury and SO<sub>2</sub> to elucidate the adsorption and migration pathways of SO<sub>2</sub> and mercury [11]. Such an in-depth study holds significant implications for effectively controlling mercury pollution in the nonferrous smelting industry.

This study aims to improve the state of global sustainable development and explore the applicability of AC for removing Hg<sup>0</sup> concerning the high temperature and high sulfur flue gas characteristics prior to the acid production process of nonferrous smelting. Firstly, the performances of AC for removing mercury at different temperatures were investigated. Kinetic simulation calculations were carried out to derive the optimal adsorption temperature window and kinetic mechanism. The impact of varying flue gas components on mercury removal was also investigated. The mechanism of SO<sub>2</sub> and O<sub>2</sub> action on the surface of AC was analyzed using X-ray photoelectron spectroscopy (XPS) and thermal desorption experiment programmed with mercury (Hg-TPD). The study examined the potential use of AC for removing mercury in the nonferrous smelting industry, offering a theoretical foundation for the widespread adoption and implementation of AC adsorption technology to enhance sustainable development.

## 2. Materials and Methods

### 2.1. Experimental Material

The AC was sourced from Shanxi Xinhua Chemical Co., Ltd. (Taiyuan, China). All the reagents were directly used without undergoing additional purification. To ensure optimal contact between the flue gas and adsorbent and to prevent excessive air resistance and disruption of airflow, the purchased large AC particles were grounded and crushed to 40–60 mesh using a sieve. The resulting AC particles were then washed with distilled water one or two times, then steamed and dried in a drying oven at 100 °C for about twenty hours for spare use. Water from a m pure HIQ water purification system (minimum of 18 MV cm) was used. The high purity N<sub>2</sub> and O<sub>2</sub> concentrations were 99.999%, and SO<sub>2</sub> was 1%.

## 2.2. Evaluation of Mercury Adsorption Performance

This experiment utilized a fixed-bed reaction system with the manufactured AC particles as the adsorbent and a series of simulated flue gases to measure the capacity of combined desulfurization and mercury removal. The fixed-bed reactor system is shown in Figure 1, which consists of a gaseous singlet mercury generation system, a fixed-bed and temperature control system, a simulated flue gas system, a gaseous singlet mercury test system, and a tail gas treatment system. The tail gas generated from this experiment had been treated and discharged to the designated site to avoid any negative environmental impact due to this study.

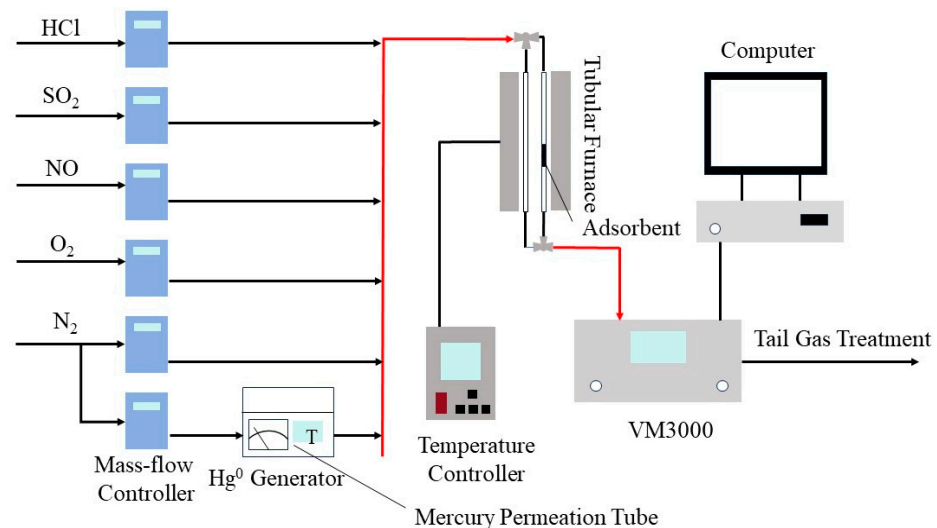


**Figure 1.** Schematic diagram of  $\text{Hg}^0$  removal experiment in fixed bed reactor.

The  $\text{Hg}^0$  removal performances of the material at different temperatures and gas compositions were preliminarily tested. The specific experimental steps are shown in Table 1. The aims of the experiments are as follows: Experiment I investigated the  $\text{Hg}^0$  removal effects of the reaction temperature using AC. These experiments were performed in an  $\text{N}_2$  atmosphere; Experiment II–IV investigated the influences of  $\text{O}_2$  and  $\text{SO}_2$  on  $\text{Hg}^0$  removal performance. Finally, Experiment V determined the  $\text{Hg}$  species and elucidated the removal mechanisms of spent  $\text{Hg}^0$  and AC by  $\text{Hg}$ -TPD.

**Table 1.** Experimental conditions for mercury removal from AC.

Experimental Groups	Gas Conditions	Temperature (°C)
I	$\text{N}_2$	60, 90, 120, 150, 180, 210
II	$\text{N}_2 + 5\% \text{O}_2$	150
III	$\text{N}_2 + 2000 \text{ ppm SO}_2$	150
IV	$\text{N}_2 + 5\% \text{O}_2 + 2000 \text{ ppm SO}_2$	150
V	II–IV + $\text{N}_2$	50–600, $10^\circ \text{C}/\text{min}$

Notes: Airflow 1.2 L/min, AC 20 mg, 40–60 mesh.

The inlet and outlet mercury concentrations can be measured online in real-time by a mercury meter, and the amount of mercury adsorbed is calculated using Equation (1):

$$Q_t = \frac{F}{m} \int_{t_1}^{t_2} (\text{Hg}_{in}^0 - \text{Hg}_{out}^0) dt \quad (1)$$

where  $Q_t$  is the amount of mercury adsorbed (mg/g),  $F$  is the simulated flue gas flow rate ( $\text{m}^3/\text{min}$ ),  $m$  is the mass of the adsorbent (g),  $t_1$  and  $t_2$  are the reaction start time and end time (min), respectively, and  $\text{Hg}_{in}^0$  and  $\text{Hg}_{out}^0$  are the inlet and outlet mercury concentrations ( $\text{mg}/\text{m}^3$ ), respectively.

The efficiency of mercury removal is calculated using Equation (2):

$$\eta = \frac{Q_t}{\frac{F}{m} \int_{t_1}^{t_2} Hg_{in}^0 dt} \quad (2)$$

where  $\eta$  is the mercury removal efficiency (%).

The pseudo-first-order kinetic model predicts the  $Hg^0$  adsorption capacity based on an ~80% breakthrough dataset. The  $Hg^0$  adsorption rate is proportional to the difference between the equilibrium capacity and the adsorbed amount at any time, as described as follows:

$$\frac{dQ_t}{dt} = k_1(Q_e - Q_t) \quad (3)$$

Equation (3) could be modified to the following equation based on the initial conditions of  $t = 0$ ,  $Q_t = 0$ :

$$Q_t = Q_e(1 - e^{-k_1 t}) \quad (4)$$

The pseudo-first-order kinetic constant ( $k_1$ ,  $\text{min}^{-1}$ ) can be determined by fitting the adsorption breakthrough curve.

Additionally, the pseudo-second-order kinetic model is also adopted to simulate the  $Hg^0$  adsorption behavior, which could be described by Equation (5):

$$\frac{dQ_t}{dt} = k_2(Q_e - Q_t)^2 \quad (5)$$

Equation (5) could be modified to the following equation based on the initial conditions of  $t = 0$ ,  $Q_t = 0$ :

$$\frac{t}{Q_t} = \frac{1}{k_2 Q_e^2} + \frac{1}{Q_e} t \quad (6)$$

where the pseudo-second-order kinetic constant ( $k_2$ ,  $\text{mg} \cdot \text{g}^{-1} \cdot \text{min}^{-1}$ ) can be determined by fitting the adsorption breakthrough curve.

### 2.3. Sample Characterization

The unique physicochemical properties of AC are essential for its good mercury removal effect. To further understand its properties, it is necessary to test and analyze the AC before and after adsorption utilizing BET surface area measurement, X-ray photoelectron spectroscopy, etc., and the results and the adsorption and desorption data will work together to provide a specific theoretical basis for the adsorption of the influencing factors and mechanisms. A physical adsorbent meter determined the specific surface area, pore volume, and pore size data (Mike ASAP 3020, Micromeritics, Norcross, GA, USA). 200 mg of the sample was weighed and degassed under a vacuum at 120 °C for 12 h, followed by  $N_2$  adsorption/desorption at −198 °C. The specific surface areas of the samples were calculated using the Horv'ath–Kawazoe (HK) model, and the pore size distribution was calculated using the density functional theory (DFT) model. The X-ray photoelectron spectrometer (ESCALAB 250Xi, Thermo Fisher Scientific, Waltham, MA, USA) was utilized with Al K $\alpha$  ( $h\nu = 1486.6$  eV) serving as the excitation source. The parameters were as follows: 150 W power, 650  $\mu\text{m}$  beam spot, 14.8 KV voltage, and 1.6 A current. The monochromatic Al K $\alpha$  charge correction was performed using contaminated carbon C1s = 284.8 eV. The full-spectrum flux was 100 eV in steps of 1 eV, whereas the narrow-spectrum flux was 20 eV in steps of 0.1 eV. Hg-TPD experiments were performed on the experimental platform. The sample was cooled to 50 °C after adsorption of Hg and purged with 1000 mL/min  $N_2$  for 80 min; then, the temperature was increased from 50 °C to 600 °C at a rate of 10 °C/min with  $N_2$  as the carrier gas.

### 3. Results and Discussion

#### 3.1. Effect of Temperature on Mercury Removal Performance

To elucidate the effect of temperature on the mercury removal performance of AC, the mercury removal performance was evaluated in the range of 60–210 °C. As shown in Figure 2a, when the adsorption temperature was 60 °C, the  $\text{Hg}^0$  adsorption performance of AC gradually decreased within 120 min. Raising the adsorption temperature was favorable to the adsorption of  $\text{Hg}^0$  onto AC. The adsorption effect becomes better when the temperature increases from 60 °C to 150 °C, reaching the highest adsorption efficiency at 150 °C. However, when the adsorption temperature was increased from 150 °C to 210 °C, the removal efficiency decreased sharply from 97.7% to 86.8%, as shown in Figure 2b, which was calculated according to Equation (2). This phenomenon illustrates that the energy provided by the temperature from 150 °C to 210 °C is not enough to make the chemical bond rupture but enough to break through the van der Waals force [16], resulting in the desorption amount greater than the adsorption amount, which is macroscopically manifested as a decrease in the amount of adsorption.

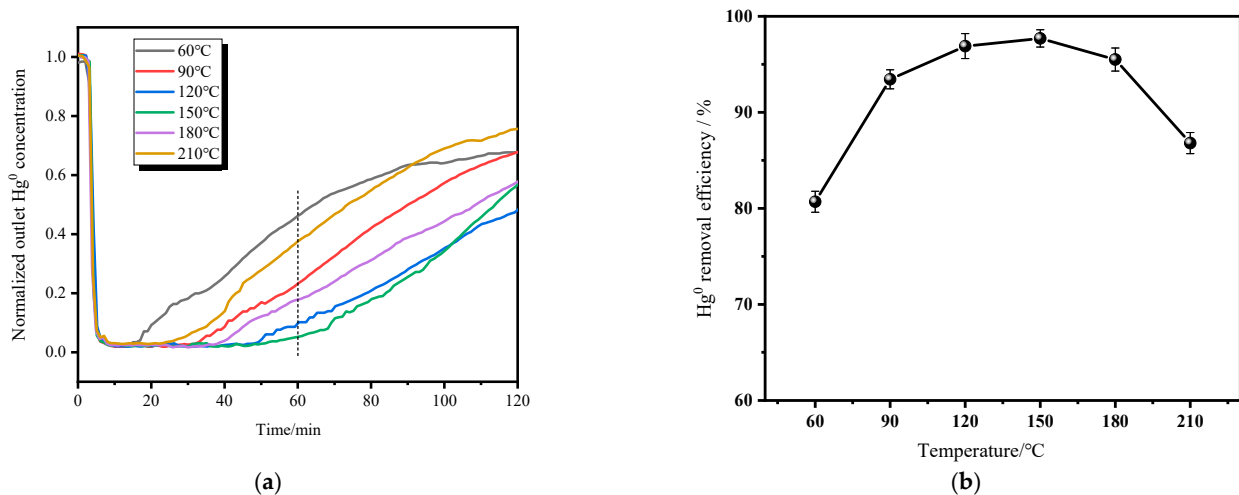


**Figure 2.** (a)  $\text{Hg}^0$  adsorption breakthrough curves of AC at 60–210 °C; (b)  $\text{Hg}^0$  removal efficiency after 120 min adsorption. Reaction conditions: flow rate = 1250 mL/min, sorbent mass = 20 mg,  $\text{Hg}^0$  concentration =  $65 \pm 5 \mu\text{g}/\text{m}^3$ ,  $\text{N}_2$  balance, and WHSV =  $3,750,000 \text{ cm}^3 \cdot \text{g}^{-1} \cdot \text{h}^{-1}$ .

Physical adsorption is a thermodynamically favorable process whereby an increase in temperature leads to a shift in the adsorption equilibrium towards desorption, reducing the quantity of  $\text{Hg}^0$  adsorbed [17]. Moreover, excessively high temperatures can detrimentally impact the active adsorption sites present on the surface of the AC, thereby diminishing its binding capacity for  $\text{Hg}^0$  and subsequently decreasing the efficiency of  $\text{Hg}^0$  adsorption [18]. Figure 2 demonstrates that when the temperature is close to 150 °C, the efficiency of mercury removal in the first 60 min is significantly higher than at other temperatures. The data presented in the figure indicates that mercury removal efficiency in the initial 60 min is notably more increased when the temperature approaches 150 °C compared to other temperatures. Considering both physical and chemical adsorption, it can be concluded that 150 °C is the optimal temperature for conducting further experimental investigations.

The adsorption capacity and adsorption efficiency curves of AC at 150 °C were calculated according to Equations (1) and (2), as shown in Figure 3. Furthermore, after approximately 4.2 h of experimentation, the penetration threshold of AC reached 85% of its adsorption capacity of 0.55 mg/g. Additionally, the rate of change in adsorption quantity gradually decreased as the adsorption process progressed.

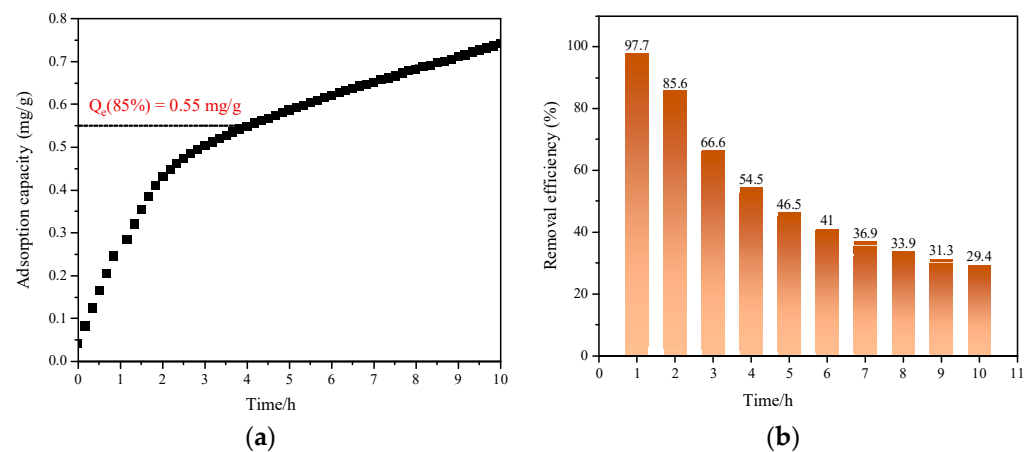


**Figure 3.** The adsorption capacity curve of AC at 150 °C: (a) Mercury adsorption amount with time; (b) Mercury adsorption efficiency with time.

Figure 3b illustrates a significant decline in adsorption efficiency within the initial 4-h period, followed by a stabilization once adsorption commenced. After 10 h of adsorption, a penetration rate of 29.4% was achieved with 20 mg of AC, corresponding to an adsorption capacity of  $742.2 \mu\text{g}\cdot\text{g}^{-1}$ . It can be inferred that the remaining void volume of the AC influences the adsorption rate. Consequently, the proposed primary and secondary kinetics assumptions were examined to investigate the applicability of first and second-order kinetics in describing the speed of the adsorption process. As shown in Figure 4a,b, the adsorption behavior of  $\text{Hg}^0$  by AC was simulated using the kinetic models of Equations (4) and (6), respectively. In the adsorption process, without changing the mercury concentration in the inlet gas, the adsorption speed can only be related to the occupancy rate of the pores. The fitting results showed that the correlation coefficient  $R^2$  of the pseudo-first-order kinetic model was as high as 0.9997, while the linear correlation coefficient  $R^2$  in the pseudo-second-order kinetic model was only 0.9688. Therefore, using the pseudo-first-order kinetic model, the adsorption rate  $K_1$  of AC on  $\text{Hg}^0$  was calculated to be  $9.29 \times 10^{-4} \text{ min}^{-1}$ .

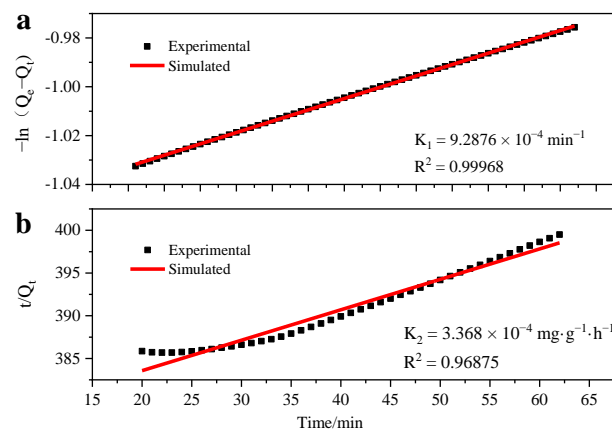


**Figure 4.** (a) represents the pseudo-first-order kinetic curve, and (b) represents the pseudo-second-order kinetic curve.

In the event of a particular mercury concentration in the inlet, the adsorption rate adheres to the pseudo-first-order kinetic equation for the quantity of void, wherein the vacuum portion is the penetration amount minus the present adsorption amount. Conversely, the adsorption rate constant exhibits a strong correlation with temperature [19]. As temperature increases, the adsorption rate accelerates; however, the desorption rate intensifies concurrently [20]. The exothermic nature of the adsorption process further

contributes to the establishment of adsorption equilibrium in the direction of desorption as the temperature rises, i.e., as the temperature increases to a certain extent, the desorption amount is more significant than the amount of adsorption, which will lead to a decrease in the capacity of AC boundary, which is in line with the results shown in Figure 2.

The adsorption performance of several typical activated carbons for  $\text{Hg}^0$  is summarized in Table 2. The adsorption capacity of AC used in this paper for  $\text{Hg}^0$  was much higher than that of the ACs reported by the previous authors. The results indicated that AC is an effective  $\text{Hg}^0$  capture agent.

**Table 2.** Adsorption capacity comparison between AC and typically reported.

Raw Material Source	Means of Treatment	Adsorption Efficiency	Adsorption Capacity ( $\mu\text{g/g}$ )	Reference
commercial cokes from Shanxi Xinhua Chemical Co., Ltd., Taiyuan, China	Separation and washing	98%	742.2	This work
Zhundong lignite	Separation and purification	91%	30.72	[12]
commercial cokes from Inner Mongolia Kexing Carbon Industry Co., Ltd., Hohhot, China	Mn-Ce impregnation	94.87%	No data	[13]
commercial cokes from Inner Mongolia Taixi Group Xingtai Coal Chemistry Co., Ltd., Alxa, China	Cu impregnation	>90%	No data	[14]
commercial cokes from Gongyi Zhongya water purification materials Co., Ltd., Gongyi, China	Co-Ce impregnation	71.07%	No data	[15]

Nonferrous metal smelting flue gas is complex, mainly containing  $\text{O}_2$ ,  $\text{SO}_2$ , and other components [21,22]. This study aimed to examine the impact of flue gas components on the efficacy of AC in removing  $\text{Hg}^0$ . Specifically, the  $\text{Hg}^0$  removal efficiencies were compared when exposed to  $\text{SO}_2$  and  $\text{O}_2$  individually, as well as under composite conditions. The results, as depicted in Figure 5, indicated that the  $\text{Hg}^0$  adsorption efficiency of AC reached 95% when tested under pure  $\text{N}_2$  conditions. The presence of  $\text{O}_2$  did not significantly affect  $\text{Hg}^0$  adsorption, as the removal efficiency remained at 95% even with its addition.

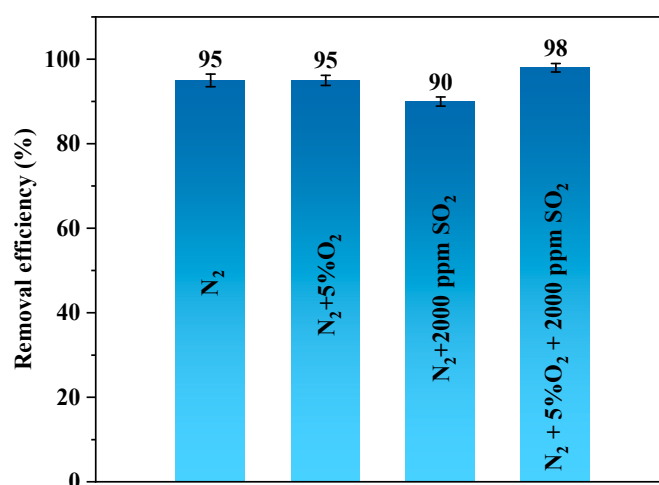


**Figure 5.** The influence of flue gas components on the  $\text{Hg}^0$  removal performance of AC.

Adding 2000 ppm SO<sub>2</sub> into pure N<sub>2</sub> decreased Hg<sup>0</sup> removal efficiency from 95% to 90%, suggesting that SO<sub>2</sub> hindered the adsorption activity of Hg<sup>0</sup> by the AC. This inhibition can be attributed to two factors [23]: (1) the competitive adsorption of SO<sub>2</sub> with Hg<sup>0</sup> on the surface of the adsorbent, and (2) the reaction of SO<sub>2</sub> with the active sites and oxygen-containing functional groups, leading to a reduction in adsorption activity [24]. Conversely, when both SO<sub>2</sub> and O<sub>2</sub> were present in the atmosphere, the Hg<sup>0</sup> removal efficiency increased from 95% to 98%, indicating that the simultaneous presence of SO<sub>2</sub> and O<sub>2</sub> facilitated Hg<sup>0</sup> removal. This may be due to (1) SO<sub>2</sub> is oxidized to SO<sub>3</sub> by the metal oxides on the adsorbent, and the SO<sub>3</sub> formed on the adsorbent surface oxidizes Hg<sup>0</sup> to Hg<sup>2+</sup>; (2) in the gas phase, SO<sub>2</sub> binds to O<sub>2</sub> and oxidizes Hg<sup>0</sup> to Hg<sup>2+</sup>; and (3) after SO<sub>2</sub> adsorption on the adsorbent, the adsorption activity of the neighboring adsorption sites is increased, which enhances the efficiency of the adsorbent [25,26]. It should be noted that although mercury removal by AC was not high, the experiments were conducted with the AC dosage as low as 20 mg. According to previous studies, mercury removal can be effectively improved by increasing the adsorbent dosage [27]. Obviously, in practical applications, the dosage of the AC will be much higher than the milligram level to ensure operational stability and long-term durability [28–30]. Therefore, it can be concluded that the AC exhibits a relatively wide range of capabilities for removing Hg<sup>0</sup> from nonferrous smelting flue gases.

### 3.2. Specific Surface Area Analysis

As shown in Figure 6a, the pristine and used AC exhibited a typical Type II isotherm curve, with the adsorption amount dramatically increasing when P/P<sup>0</sup> escaped zero, indicating the abundance and uniformity of the micropores, which were the primary characteristics of coke [31]. The HK model was adopted to characterize the micropores of the AC, and the results further supported the enrichment of micropores in pristine and used AC (Figure 6b). In addition, a relatively wide hysteresis loop was observed for P/P<sup>0</sup>, with values ranging from 0.5 to 1.0. This suggested the co-existence of meso- and macro-pores, which could contribute to the favorable structure formation observed in the pristine AC samples (Figure 6b) [32]. The surface area of pristine AC reached 231.45 m<sup>2</sup>/g (Table 3) and could be attributed to the enrichment of the pores and the hierarchical nature of its structures. Consequently, pristine AC was more favorable for the diffusion of Hg<sup>0</sup> [20,33].

The surface physical properties of the AC before and after adsorption under different flue gas conditions were obtained, including the specific surface area, pore volume, and average pore diameter, as shown in Table 3.

Based on the data presented in Table 3, it was evident that the specific surface area of the AC, when exposed to Hg<sup>0</sup> in pure N<sub>2</sub>, remained unchanged, while the pore volume and average pore diameter experienced a slight reduction. The introduction of SO<sub>2</sub> further diminished the surface's physical properties. Notably, the sample subjected to both SO<sub>2</sub> and O<sub>2</sub> exhibited the most significant decline in surface physical properties, thereby substantiating the notion that the presence of O<sub>2</sub> facilitated the synergistic removal of both SO<sub>2</sub> and Hg<sup>0</sup> by the AC.

**Table 3.** Surface Physical Properties of the AC.

Samples	Specific Surface Areas (m <sup>2</sup> /g)	Pore Volume (cm <sup>3</sup> /g)	Average Pore Diameter (nm)
Fresh coke	231.45	0.055	3.43
Used coke N <sub>2</sub>	231.46	0.054	3.26
Used coke N <sub>2</sub> + 2000 ppm SO <sub>2</sub>	213.69	0.052	3.28
Used coke N <sub>2</sub> + 5% O <sub>2</sub> + 2000 ppm SO <sub>2</sub>	209.41	0.051	3.29

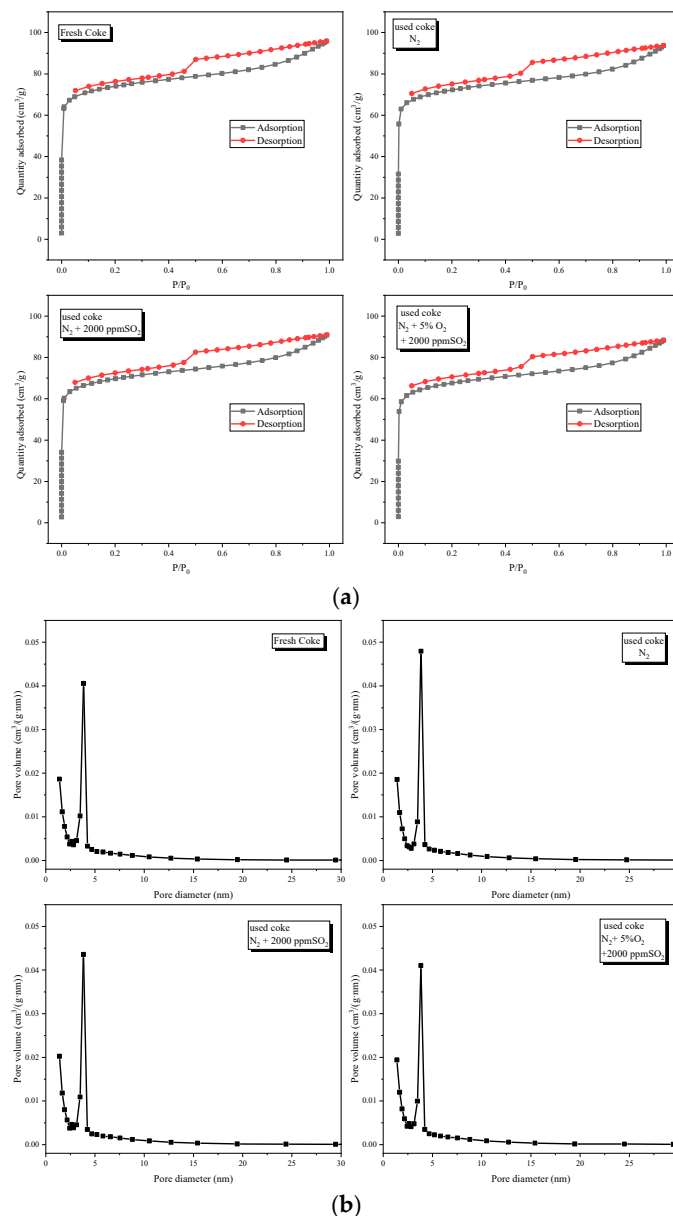
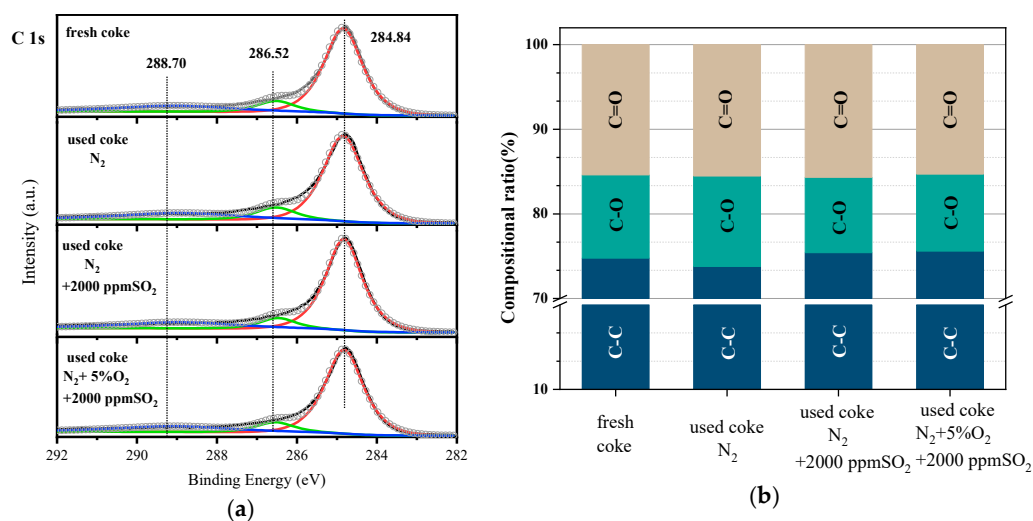


**Figure 6.** (a) N<sub>2</sub> adsorption–desorption patterns; (b) pore distributions of pristine and used ACs.

### 3.3. Mechanism Analysis

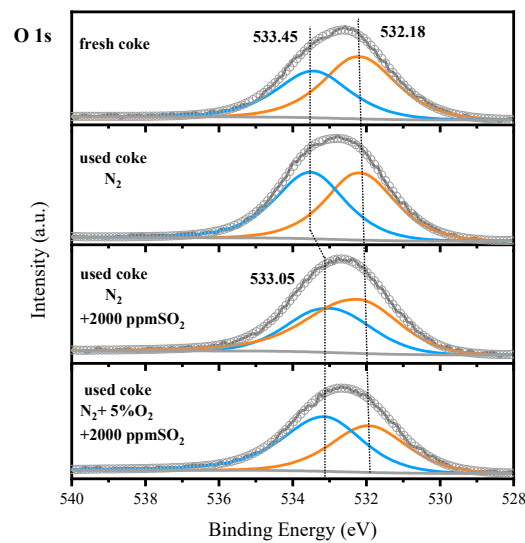
To investigate the mercury fugitive morphology and adsorption mechanism on the AC, the chemical state of the surface elements before and after the reaction was analyzed by XPS characterization.

Figure 7a demonstrated the split-peak fitting of the XPS spectra of C 1s, resulting in three peaks situated at 284.8 eV, 286.5 eV, and 288.7 eV, corresponding to C-C bonded, C-O bonded, and C=O bonded, respectively [34]. The figure illustrated that the positions of the three C peaks remained unaltered before and after the adsorption of Hg<sup>0</sup>, regardless of the atmospheric conditions. Figure 7b displayed a histogram illustrating the proportions of the areas of the three peaks, indicating that the relative contents of C-C bonds, C-O bonds, and C=O bonds in the AC samples remained relatively stable. It demonstrated that element C was not involved in the adsorption process of Hg<sup>0</sup>.



**Figure 7.** XPS patterns of the adsorbents: (a) C 1s; (b) Changes in the relative proportions of different C bonds in C 1s.

Figure 8 demonstrated the peak splitting of the O 1s XPS spectrum, resulting in two distinct peaks at 533.45 eV and 532.18 eV, corresponding to the chemisorbed oxygen ( $O_{\alpha}$ ) and the lattice oxygen ( $O_{\beta}$ ), respectively [35]. According to existing literature,  $O_{\alpha}$  and  $O_{\beta}$  were categorized as surface active oxygen and could actively participate in oxidation reactions [36]. Based on the depicted figure, it was evident that the peak position of  $O_{\beta}$  remained relatively unchanged before and after the utilization of the AC. Conversely, the peak position of  $O_{\alpha}$  exhibited a discernible shift towards lower binding energy after the introduction of  $SO_2$ , suggesting that the  $O_{\alpha}$  site, where  $SO_2$  was anchored, exerted a conspicuous electron-donating influence, thereby significantly augmenting the electron cloud density of  $O_{\alpha}$ . The XPS characterization yielded elemental content data, which enabled the acquisition of the relative carbon contents of oxygen, sulfur, and mercury, both before and following the implementation of the AC, as illustrated in Figure 9. As can be seen from the figure, the relative content of O remained constant before and after the utilization of the AC in various atmospheres. Additionally, the introduction of  $SO_2$  in the atmosphere resulted in the emergence of S on the AC surface, while the inclusion of  $O_2$  facilitated the deposition of  $SO_2$  on the AC surface. Notably, the presence of  $N_2$  and  $SO_2$  alone led to a substantial reduction in the corresponding mercury element content, indicating that  $SO_2$  competed with gaseous monomers of mercury for adsorption and inhibited the adsorption of  $Hg^0$ . More  $SO_2$  was absorbed after the addition of  $O_2$ , which proved that  $O_2$  could promote the generation of  $SO_3$  from part of  $SO_2$  and enhance the chemisorption of sulfur. Furthermore, introducing  $O_2$  resulted in an augmentation of  $Hg^0$  adsorption, aligning with the findings in Figure 5. Two potential mechanisms can account for this phenomenon: (1)  $O_2$  generates oxygen-containing functional groups on the surface of the AC, thereby directly enhancing the chemisorption capacity of gaseous mercury monomers; (2) the oxygen-containing functional groups initially interact with  $SO_2$ , leading to the production of  $SO_3$  and subsequent oxidation of mercury. Oxygen-containing functional groups possess greater polarity and are theoretically inclined to react with the polar molecule  $SO_2$  preferentially, so the second possibility is more probable.



**Figure 8.** XPS patterns of the adsorbents O1s.

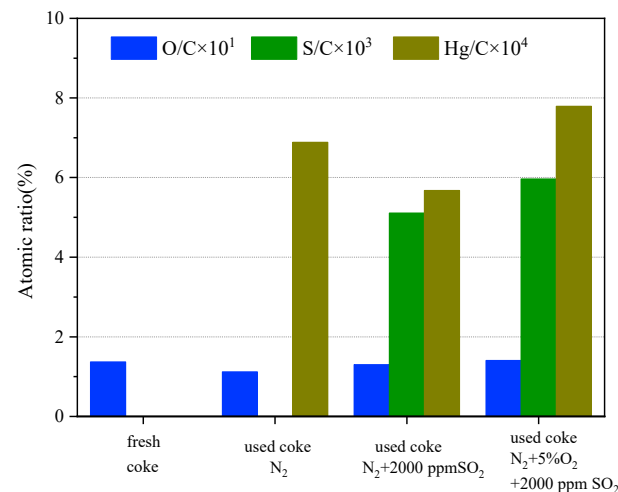


**Figure 9.** Comparison of the relative carbon content of the three elements oxygen, sulfur, and mercury before and after the use of the AC.

It is possible to identify the mercury species by the method of thermal desorption [24,37,38]. The four cokes used in different atmospheres after mercury adsorption were analyzed for use as fingerprints, as shown in Figure 10. It was obvious that the position of Hg-TPD peaks of the AC in N<sub>2</sub>, O<sub>2</sub>, and SO<sub>2</sub> atmospheres was located between 310–320 °C, which was attributed to the HgO decomposition peak; the position of Hg-TPD peaks of the AC in O<sub>2</sub> + SO<sub>2</sub> atmospheres was situated at 293.4 °C, which corresponds to the HgSO<sub>4</sub> detachment peak [37]. The Hg-TPD test results indicated that the adsorption products of Hg under the three atmospheres of N<sub>2</sub>, O<sub>2</sub>, and SO<sub>2</sub> were dominated by HgO, and HgSO<sub>4</sub> dominated the product of Hg<sup>0</sup> under the SO<sub>2</sub> + O<sub>2</sub> atmosphere. Combined with the previous Figure 8 analysis, it can be further deduced that under the SO<sub>2</sub> + O<sub>2</sub> atmosphere, the oxygen-containing functional group first reacts with SO<sub>2</sub> to produce SO<sub>3</sub> and then oxidizes Hg, and the oxidation product is HgSO<sub>4</sub>.

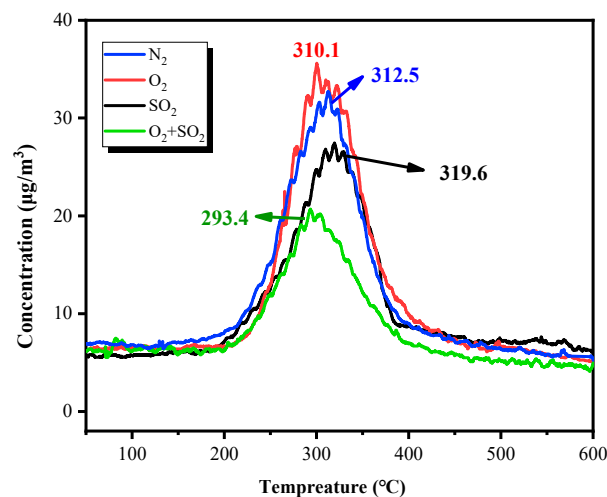


**Figure 10.** The Hg-TPD pattern of spent cokes.

As shown in Figure 11, the temperature segments in the adsorption process were integrated to obtain the desorption amount in different temperature segments. Based on the increase in mercury release in each temperature interval, it is possible to see in which temperature interval the release of mercury is most concentrated, and the optimal temperature interval for mercury release can be deduced. As can be seen from Figure 11, the desorption amount raised slightly at 0–200 °C and proliferated at 200–400 °C and then stayed at a higher level, which indicated that the higher the temperature was, the better the desorption effect was, while the desorption capacity no longer improved drastically with the rise of temperature after reaching 400 °C.

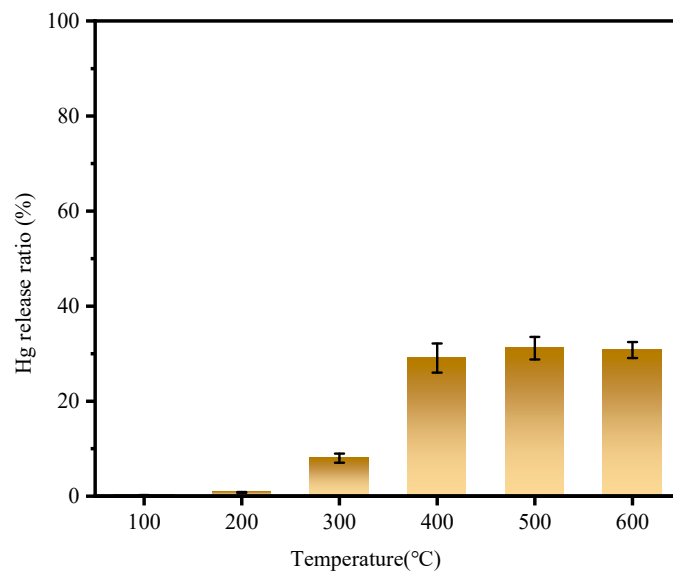


**Figure 11.** Hg release ratio of spent AC at different temperatures.

#### 4. Conclusions

This paper investigates the suitability of the AC removal process for  $\text{Hg}^0$  in nonferrous smelting flue gas before the acid production process, considering the high temperature and high sulfur flue gas characteristics. The adsorption performance of the AC was evaluated, and the results indicated that the highest adsorption efficiency of  $\text{Hg}^0$  was achieved at an adsorption temperature of 150 °C. Furthermore, the adsorption performance of the AC at various temperatures and the results of kinetic simulation demonstrated that the adsorption of  $\text{Hg}^0$  by the AC primarily involved physical adsorption rather than chemical adsorption.

The impact of various flue gas components, namely  $\text{SO}_2$  and  $\text{O}_2$ , on the performance of AC in removing  $\text{Hg}^0$  was investigated. The results indicated that  $\text{O}_2$  had a negligible influence on  $\text{Hg}^0$  adsorption compared to pure  $\text{N}_2$ , while  $\text{SO}_2$  hindered the adsorption activity of AC towards  $\text{Hg}^0$ . Interestingly, the simultaneous presence of  $\text{SO}_2$  and  $\text{O}_2$  facilitated the removal of  $\text{Hg}^0$ . XPS analysis revealed that carbon (C) did not participate in the adsorption process of  $\text{Hg}^0$ , whereas  $\text{SO}_2$  acted as the anchoring point for AC. Specifically, the anchoring site of  $\text{SO}_2$  was identified as the  $\text{O}_\alpha$  site. When  $\text{SO}_2$  and  $\text{O}_2$  were present simultaneously, the oxygen-containing functional groups reacted with  $\text{SO}_2$  first to generate  $\text{SO}_3$  and then oxidized mercury, and the product was  $\text{HgSO}_4$ .  $\text{HgO}$  dominated the adsorption products of the monomers of mercury under the atmosphere of pure  $\text{N}_2$  and the addition of  $\text{SO}_2$  and  $\text{O}_2$  alone.

Despite the advantages and potential applications of AC adsorption of mercury technology, further research and improvement are necessary to address existing issues, enhance its technical proficiency, and optimize its economic benefits. This will enable sustainable development in mercury emission control and facilitate the dissemination and implementation of AC adsorption of mercury technology by offering guidance and recommendations.

**Author Contributions:** Conceptualization, Y.Z. and T.Y.; methodology, Y.Z.; software, G.L.; validation, J.J., L.Z. and Y.Z.; formal analysis, Y.Z.; investigation, L.Z.; resources, Y.Z. and T.Y.; data curation, J.J.; writing—original draft preparation, Y.Z.; writing—review and editing, G.L.; visualization, Y.Z.; supervision, T.Y.; project administration, T.Y.; funding acquisition, Y.Z. and T.Y. All authors have read and agreed to the published version of the manuscript.

**Funding:** This research was funded by “Basic Research Business Fund Grant Program for University of Science and Technology Beijing, grant number 06500227”, “Fundamental Research Funds for the Central Universities, grant number FRF-TP-22-091A1”; and “Interdisciplinary Research Project for Young Teachers of USTB (Fundamental Research Funds for the Central Universities), grant number FRF-IDRY-22-010”.

**Institutional Review Board Statement:** Not applicable.

**Informed Consent Statement:** Not applicable.

**Data Availability Statement:** Data available on request due to restrictions (e.g., privacy or ethics).

**Conflicts of Interest:** The authors declare no conflicts of interest.

## References

1. Yang, X.; Gong, C.; Guan, Y.; Li, J.; Li, F.; Peng, C.; Wu, J.; Cui, T.; Xiang, S.; Gao, Y. Novel bimetallic chalcogenide adsorbents for elemental mercury removal from flue gas: A review. *Fuel* **2023**, *344*, 128081. [CrossRef]
2. Luskiewicz, D.; Jedrusik, M.; Swierczok, A.; Kobylanska-Pawlisz, M. Effect of addition of sulphide based additive to WFGD slurry on mercury removal from flue gas. *Energy* **2023**, *270*, 126953. [CrossRef]
3. UNEP. Global Mercury Assessment. 2018. Available online: <https://www.unep.org/resources/publication/global-mercury-assessment-2018> (accessed on 28 November 2023).
4. Zhao, Y.; Zhong, H.; Zhang, J.; Nielsen, C.P. Evaluating the effects of China’s pollution controls on inter-annual trends and uncertainties of atmospheric mercury emissions. *Atmos. Chem. Phys.* **2015**, *15*, 4317–4337. [CrossRef]
5. Wu, Q.; Wang, S.; Zhang, L.; Hui, M.; Wang, F.; Hao, J. Flow Analysis of the Mercury Associated with Nonferrous Ore Concentrates: Implications on Mercury Emissions and Recovery in China. *Environ. Sci. Technol.* **2016**, *50*, 1796–1803. [CrossRef] [PubMed]
6. Liao, Y.; Xu, H.; Liu, W.; Ni, H.; Zhang, X.; Zhai, A.; Quan, Z.; Qu, Z.; Yan, N. One Step Interface Activation of ZnS Using Cupric Ions for Mercury Recovery from Nonferrous Smelting Flue Gas. *Environ. Sci. Technol.* **2019**, *53*, 4511–4518. [CrossRef] [PubMed]
7. Yang, S.; Liu, C.; Wang, P.; Yi, H.; Shen, F.; Liu, H.  $\text{Co}_9\text{S}_8$  nanoparticles-embedded porous carbon: A highly efficient sorbent for mercury capture from nonferrous smelting flue gas. *J. Hazard. Mater.* **2021**, *412*, 124970–124978. [CrossRef]
8. Zheng, W.; Yang, Z.; Yang, J.; Qu, W.; Feng, Y.; Jiang, S.; Zhao, S.; Shih, K.; Li, H. Favorably adjusting the pore characteristics of copper sulfide by template regulation for vapor-phase elemental mercury immobilization. *J. Mater. Chem. A* **2022**, *10*, 10729–10737. [CrossRef]
9. Zhou, X.-h.; Zhang, S.-f.; Wei, Y.-y.; Sher, F.; Li, Y.; Yu, W.-z.; Wen, L.-y. Preparation of active coke combining coal with biomass and its denitrification performance. *J. Iron Steel Res. Int.* **2021**, *28*, 1203–1211. [CrossRef]

10. Zhang, J.; Li, C.; Du, X.; Li, S.; Huang, L. Recycle of waste activated coke as an efficient sorbent for Hg<sup>0</sup> removal from coal-fired flue gas. *Fuel* **2022**, *324*, 124645–124654. [[CrossRef](#)]
11. Zhang, H.; Wang, T.; Zhang, Y.; Wang, J.; Sun, B.; Pan, W.-P. A review on adsorbent/catalyst application for mercury removal in flue gas: Effect of sulphur oxides (SO<sub>2</sub>, SO<sub>3</sub>). *J. Clean. Prod.* **2020**, *276*, 124220–124238. [[CrossRef](#)]
12. An, D.; Sun, X.; Cheng, X.; Cui, L.; Zhang, X.; Zhao, Y.; Dong, Y. Investigation on mercury removal and recovery based on enhanced adsorption by activated coke. *J. Hazard. Mater.* **2020**, *384*, 121354. [[CrossRef](#)] [[PubMed](#)]
13. Xie, Y.; Li, C.; Zhao, L.; Zhang, J.; Zeng, G.; Zhang, X.; Zhang, W.; Tao, S. Experimental study on Hg<sup>0</sup> removal from flue gas over columnar MnOx-CeO<sub>2</sub>/activated coke. *Appl. Surf. Sci.* **2015**, *333*, 59–67. [[CrossRef](#)]
14. Zhao, B.; Yi, H.; Tang, X.; Li, Q.; Liu, D.; Gao, F. Copper modified activated coke for mercury removal from coal-fired flue gas. *Chem. Eng. J.* **2016**, *286*, 585–593. [[CrossRef](#)]
15. Chen, J.; Li, C.; Li, S.; Lu, P.; Gao, L.; Du, X.; Yi, Y. Simultaneous removal of HCHO and elemental mercury from flue gas over Co-Ce oxides supported on activated coke impregnated by sulfuric acid. *Chem. Eng. J.* **2018**, *338*, 358–368. [[CrossRef](#)]
16. Xiao, R.; Zhang, Y.; Wei, S.; Chuai, X.; Cui, X.; Xiong, Z.; Zhang, J.; Zhao, Y. A high efficiency and high capacity mercury adsorbent based on elemental selenium loaded SiO<sub>2</sub> and its application in coal-fired flue gas. *Chem. Eng. J.* **2023**, *453*, 139946. [[CrossRef](#)]
17. Ho, T.C.; Shetty, S.; Chu, H.W.; Lin, C.J.; Hopper, J.R. Simulation of mercury emission control by activated carbon under confined-bed operations. *Powder Technol.* **2008**, *180*, 332–338. [[CrossRef](#)]
18. Liu, Z.; Sun, P.; Chen, S.; Shi, L. Research on Mercury Emissions Regularity and Adsorbing Mercury by Activated Carbon in Coal-fired Power Plants. *Adv. Mater. Res.* **2011**, *284–286*, 301–304. [[CrossRef](#)]
19. Graydon, J.W.; Zhang, X.; Kirk, D.W.; Jia, C.Q. Sorption and stability of mercury on activated carbon for emission control. *J. Hazard. Mater.* **2009**, *168*, 978–982. [[CrossRef](#)]
20. Yang, Y.; Liu, J.; Wang, Z.; Long, Y.; Ding, J. Interface reaction activity of recyclable and regenerable Cu-Mn spinel-type sorbent for Hg<sup>0</sup> capture from flue gas. *Chem. Eng. J.* **2019**, *372*, 697–707. [[CrossRef](#)]
21. Sodeno, R. Projected global mercury supply, demand, and excess to 2050 based on impacts of the Minamata Convention. *J. Mater. Cycles Waste Manag.* **2023**, *25*, 3608–3624. [[CrossRef](#)]
22. Cao, S.; Zhang, L.; Zhang, Y.; Wang, S.; Wu, Q. Impacts of Removal Compensation Effect on the Mercury Emission Inventories for Nonferrous Metal (Zinc, Lead, and Copper) Smelting in China. *Environ. Sci. Technol.* **2022**, *56*, 2163–2171. [[CrossRef](#)] [[PubMed](#)]
23. Sun, X.; Huang, W.; Ji, L.; Xu, H.; Qu, Z.; Yan, N. Establishing a self-supporting system of H<sub>2</sub>S production from SO<sub>2</sub> with induced catalytic reduction process for mercury capture with super-large enrichment. *Chem. Eng. J.* **2023**, *459*, 141493–141503. [[CrossRef](#)]
24. Zhang, S.; Dang, J.; Diaz-Somoano, M.; Zhang, Q. Theoretical insight into the influence of SO<sub>2</sub> on the adsorption and oxidation of mercury over the MnO<sub>2</sub> surface. *Appl. Surf. Sci.* **2023**, *626*, 157216. [[CrossRef](#)]
25. Gani, A.; Wattimena, Y.; Erdiwansyah; Mahidin; Muhibbuddin; Riza, M. Simultaneous sulfur dioxide and mercury removal during low-rank coal combustion by natural zeolite. *Heliyon* **2021**, *7*, e07052–e07058. [[CrossRef](#)]
26. Li, H.; Peng, X.; An, M.; Zhang, J.; Cao, Y.; Liu, W. Negative effect of SO<sub>2</sub> on mercury removal over catalyst/sorbent from coal-fired flue gas and its coping strategies: A review. *Chem. Eng. J.* **2023**, *455*, 140751. [[CrossRef](#)]
27. Hu, C.; Zhou, J.; Luo, Z.; Gao, H.L.; Wang, Q.H.; Cen, K.F. Factors affecting amount of activated carbon injection for flue gas mercury control. *J. Chem. Ind. Eng.* **2005**, *56*, 2172–2177.
28. Zeng, H.; Wang, X.; Li, S.; Xu, L. Experimental research of removing mercury from flue gas by activated carbon fibers. *J. Huazhong Univ. Sci. Technol. Nat. Sci.* **2006**, *34*, 1–4.
29. Goci, M.C.; Leudjo Taka, A.; Martin, L.; Klink, M.J. Chitosan-Based Polymer Nanocomposites for Environmental Remediation of Mercury Pollution. *Polymers* **2023**, *15*, 482. [[CrossRef](#)]
30. Lee, J.C.; Park, S.-W.; Kim, H.S.; Alam, T.; Lee, S.Y. Oxidation Enhancement of Gaseous Elemental Mercury Using Waste Steel Slag under Various Experimental Conditions. *Sustainability* **2023**, *15*, 1406. [[CrossRef](#)]
31. Dou, Z.; Wang, Y.; Liu, Y.; Zhao, Y.; Huang, R. Enhanced adsorption of gaseous mercury on activated carbon by a novel clean modification method. *Sep. Purif. Technol.* **2023**, *308*, 122885–122896. [[CrossRef](#)]
32. Voigt, C.; Schramm, A.; Hubalkova, J.; Brachhold, N.; Giesche, H.; Aneziris, C.G. Impact of carbon binders and carbon fillers on mercury intrusion and extrusion porosimetry of carbon-bonded alumina. *J. Eur. Ceram. Soc.* **2022**, *42*, 6264–6274. [[CrossRef](#)]
33. Zhou, Y.; Li, S.; Bai, Y.; Long, H.; Cai, Y.; Zhang, J. Joint Characterization and Fractal Laws of Pore Structure in Low-Rank Coal. *Sustainability* **2023**, *15*, 9599. [[CrossRef](#)]
34. Sivakumari, G.; Rajarajan, M.; Senthilvelan, S. Microwave-assisted synthesis and characterization of activated carbon-zirconium-incorporated CeO<sub>2</sub> nanocomposites for photocatalytic and antimicrobial activity. *Res. Chem. Intermed.* **2023**, *49*, 3539–3561. [[CrossRef](#)]
35. Fan, Y.; Wang, X.; Li, L.; Tan, J. High Resolution XPS Quantitative Study on Surface Elements and Chemical States of Novel Carbon Materials. *Chemistry* **2023**, *86*, 1018–1023.
36. Li, J.; Nolan, M.; Detavernier, C. A step toward correct interpretation of XPS results in metal oxides: A case study aided by first-principles method in ZnO. *J. Chem. Phys.* **2023**, *159*, 34702–34713. [[CrossRef](#)]

37. Rumayor, M.; Diaz-Somoano, M.; Lopez-Anton, M.A.; Martinez-Tarazona, M.R. Mercury compounds characterization by thermal desorption. *Talanta* **2013**, *114*, 318–322. [[CrossRef](#)]
38. Rumayor, M.; Gallego, J.R.; Rodríguez-Valdés, E.; Díaz-Somoano, M. An assessment of the environmental fate of mercury species in highly polluted brownfields by means of thermal desorption. *J. Hazard. Mater.* **2017**, *325*, 1–7. [[CrossRef](#)]

**Disclaimer/Publisher’s Note:** The statements, opinions and data contained in all publications are solely those of the individual author(s) and contributor(s) and not of MDPI and/or the editor(s). MDPI and/or the editor(s) disclaim responsibility for any injury to people or property resulting from any ideas, methods, instructions or products referred to in the content.